Available online at www.sciencedirect.com
ScienceDirect
Catalysis Today 131 (2008) 146–155
CATALYSIS TODAY
www.elsevier.com/locate/cattod

Catalytic performance of $Ni/CeO_2/Al_2O_3$ modified with noble metals in steam gasification of biomass

Jin Nishikawa, Kazuya Nakamura, Mohammad Asadullah, Tomohisa Miyazawa, Kimio Kunimori, Keiichi Tomishige *

Institute of Materials Science, University of Tsukuba, 1-1-1 Tennodai, Tsukuba, Ibaraki 305-8573, Japan

Available online 26 November 2007

Abstract

In the steam gasification of biomass, the additive effect of noble metals such as Pt, Pd, Rh and Ru to the $Ni/CeO_2/Al_2O_3$ catalyst was investigated. Among these noble metals, the addition of Pt was most effective even when the loading amount of added Pt was as small as 0.01 wt.%. In addition, the catalyst characterization suggests the formation of the Pt–Ni alloy over the $Pt/Ni/CeO_2/Al_2O_3$.

Keywords: Steam gasification; Steam reforming; Biomass; Tar; Coke; Regeneration

1. Introduction

Biomass can be an abundantly available and renewable energy resource. Conversion of biomass to synthesis gas and hydrogen contributes to the environmental protection by the decrease of CO_2 emission. This is because the synthesis gas can be converted into clean liquid fuels, such as methanol, and Fischer–Tropsch oil, and hydrogen is a promising energy carrier in the future. One of the conventional methods for the production of synthesis gas and hydrogen from biomass is non-catalytic gasification with air [1]. The demerit of this non-catalytic gasification is high reaction temperature above 1273 K, leading to the decrease in the total energy efficiency of the process [2]. However, the decrease of tar content in the product gas demands high reaction temperature since tar can cause some problems in the utilization of the product gas to the power generation and chemical conversion [2,3]. Although dolomite, olivine, and silica sand have been used to decrease the tar content, the effect was not so significant and the reaction temperature was almost at the same level as that of non-catalytic gasification [4]. The utilization of metal catalysts in the biomass gasification system is an effective approach to reduce the tar content [4–6]. In most cases, steam reforming Ni catalysts, which are commercially available, have been tested, and it has been pointed out that the catalyst deactivation due to coke deposition can be one of serious problems [7–10]. Our group has reported that $Rh/CeO_2/SiO_2$ exhibited much higher performance in the gasification of cellulose and biomass than conventional steam reforming Ni catalyst and dolomite at lower reaction temperature than usual, where the tar content decreased drastically and the amount of carbon deposition was very small even at the temperature as low as 823 K [4–13].

From the practical viewpoints, the gasification of biomass with air gives the gaseous fuel diluted with nitrogen, which is originated from air as a gasifying agent. Therefore, the concentration of the gaseous fuel from the biomass gasification is rather low, which can decrease the energy efficiency in the utilization of the product gas. On the other hand, the external heating is not necessary in the biomass gasification with air if the amount of oxygen is adjusted to autothermal conditions. On the other hand, the biomass can also be gasified with steam, and this process corresponds to steam gasification or steam reforming. In the steam gasification of biomass, since air is not introduced to the reactor, the product gas is not diluted with nitrogen at all. This can increase the efficiency in the utilization of the product gas. However, this process demands the external heating. In this case, this negative factor can cancel the positive aspect of gaseous products with high concentration.

It has also been reported that $Rh/CeO_2/SiO_2$ was effective in steam gasification of biomass [4,14,15]. However, the catalyst

* Corresponding author. Tel.: +81 298 53 5030; fax: +81 298 53 5030.
E-mail address: tomi@tulip.sannet.ne.jp (K. Tomishige).

0920-5861/$ – see front matter
doi:10.1016/j.cattod.2007.10.066

has problems in high cost and limited availability originated from the usage of Rh. Another promising candidate of active components is Ni. As mentioned above, since it has been known that the problem of Ni catalysts in the syngas production process is coke deposition [16–19], it is necessary to develop the catalyst with high resistance to coke deposition. Development of metal catalysts for steam gasification of biomass model compounds [15,20–24] and biomass itself [25–27] has been carried out. Recently, we have investigated coke deposition behavior over various oxides supported Ni catalysts in the steam gasification. It is characteristic that Ni/CeO_2 was effective to the suppression of coke deposition and Ni/Al_2O_3 exhibited high activity in steam reforming of tar [28]. Furthermore, we investigated the catalyst development by the combination of CeO_2 with Al_2O_3. We compared the performance on $Ni/CeO_2/Al_2O_3$ catalysts prepared by co-impregnation and sequential impregnation methods in the steam gasification of biomass [29,30]. It was found that the combination of CeO_2 and Al_2O_3 was effective as a support of Ni catalysts, and it decreased the tar and coke yields simultaneously. In particular, the $Ni/CeO_2/Al_2O_3$ catalyst prepared by the co-impregnation method was much more effective than that by the sequential impregnation method. Based on the characterization results, the interaction between Ni metal particles and CeO_2 is stronger on the catalyst prepared by the co-impregnation method, on which the composite of Ni metal and CeO_2 is formed. It is suggested that the interface between Ni metal and CeO_2 can be important in high performance of tar removal and the suppression of coke formation. In this article, we attempted to enhance the catalytic performance by the modification of the $Ni/CeO_2/Al_2O_3$ with a small amount of noble metals such as Pt, Rh, Ru and Pd.

2. Experimental

2.1. Catalyst preparation

The $Ni/CeO_2/Al_2O_3$ catalysts were prepared by a co-impregnation method using the mixed aqueous solution of $Ni(NO_3)_2{\cdot}6H_2O$ and $Ce(NH_4)_2(NO_3)_6$. Before the impregnation, Al_2O_3 (JRC-ALO-1, Catalysis Society of Japan, 143 $m^2\,g^{-1}$, grain size 2–3 mm) was calcined in air at 1423 K to change from γ-Al_2O_3 to α-Al_2O_3. After that, it was crushed and sieved to particle sizes between 0.25 and 0.6 mm. The co-impregnation was carried out by the incipient wetness method. After the impregnation, the sample was dried at 383 K for 12 h followed by the calcination at 773 K for 3 h under air atmosphere. On the other hand, the CeO_2/Al_2O_3 was also prepared by the incipient wetness method using the aqueous solution of $Ce(NH_4)_2(NO_3)_6$ and the Al_2O_3. After it was dried at 383 K for 12 h, it was calcined at 773 K for 3 h under air atmosphere. Noble metals such as Pt, Pd, Rh and Ru were loaded on the $Ni/CeO_2/Al_2O_3$ and the CeO_2/Al_2O_3 by the incipient wetness method using the aqueous solution of $Pt(NO_2)_2(NH_3)_2$, $Pd(NO_3)_2$, $Rh(NO_3)_3$ and $Ru(NO)(NO_3)_3$. After this procedure, the samples were dried at 383 K for 12 h, followed by the calcination at 773 K for 3 h under air atmosphere. These catalysts thus obtained are denoted as $M/Ni/CeO_2/Al_2O_3$ and $M/CeO_2/Al_2O_3$ (M = Pt, Pd, Rh and Ru). All these catalysts were sieved again to granules with the size of 0.25–0.6 mm. The loading amount of Ni was 4 wt.% when unindicated and 12 wt.%, and that of CeO_2 was 30 wt.%. The loading amount of Pd, Rh was 0.1 wt.%, and that of Ru was 0.5 wt.%, and that of Pt was 0.1, 0.03 and 0.01 wt.%.

2.2. Biomass

Cedar wood was ground with a ball mill to about 0.1–0.3 mm size. The moisture content of the cedar wood was 9.2%. The dry-based composition by weight was C 51.1%, H 5.9%, O 42.5%, N 0.1%, and ash 0.3%. The elemental analysis was carried out by the Japan Institute of Energy.

2.3. Activity test of steam gasification of biomass

Steam gasification of biomass was carried out in a laboratory-scale continuous feeding dual-bed reactor. The reactor contained the primary bed for pyrolysis of biomass and accumulation of solid products in the pyrolysis reaction such as char and ash. The pyrolysis products in the gas phase at reaction temperature can include tar, and they were introduced to the secondary catalyst bed. The structure of the reactor has been described in our previous reports, and the details of the procedure for catalytic performance evaluation in the steam gasification of cedar have been already described [29,30]. The biomass feeder consisted of a conical glass vessel with a screw valve at the bottom, allowing continuous feeding of biomass particles by vibrating the vessel with an electric vibrator. Nitrogen was used for transporting the biomass particles to the primary bed.

Feeding rate of gases, steam and biomass is described in each result. In the reaction, carbon-containing solid byproducts were observed. Char originated from the pyrolysis of the cedar was accumulated in the primary bed. On the other hand, the solid carbon deposited on the catalysts is called coke. The method for determining char and coke amount was the same as that in our previous reports [29–31]. The reaction temperature was controlled by the thermocouple positioned outside the reactor near the catalyst bed. The tests were carried out under atmospheric pressure by using 1 g of catalyst. We evaluated the catalytic performance over the catalysts with and without H_2 reduction pretreatment. The effluent gas was collected by a syringe and analyzed by gas chromatograph (GC). The concentration of CO, CO_2 and CH_4 was determined by FID-GC equipped with a methanator and that of H_2 was determined by TCD-GC. The flow rate of the gas was measured by a soap membrane meter. The yield of carbon-containing gaseous products is calculated by the ratio of the formation rate to the total carbon supplying rate of the biomass. The yield of coke and char is estimated by the ratio of total amount of CO_2 + CO formed in the combustion after the reaction test to the total carbon amount in fed biomass. As a result, we can measure the yield of gaseous products and solid products (coke and char). On the other hand, it is difficult to determine the tar amount

precisely. This is because tar is easily condensable in the reactor systems and a part of tar cannot be collected. We estimated the tar yield by subtraction of gaseous and solid product yields from the total as (100–C-conv. (%)–coke yield (%)–char yield (%)). In addition, we used the formation rate of $CO + H_2 + 4CH_4$ for the comparison, where four times of CH_4 is based on the reaction formula of $CH_4 + H_2O \rightarrow CO + 3H_2$. This is because the yield of the flammable gases is related to the energy efficiency in the utilization of biomass to power generation as well as the chemical utilization of produced synthesis gas.

2.4. Catalyst characterization

Surface area of catalysts was measured by BET method with Gemini (Micromeritics). Chemisorption of H_2 was carried out in a high-vacuum system by a volumetric method. Before H_2 adsorption measurement, the catalysts were treated in H_2 at 773 K for 0.5 h. H_2 adsorption was performed at room temperature. Gas pressure at adsorption equilibrium was about 1.1 kPa. The sample weight was about 0.2 g. The dead volume of the apparatus was about 60 cm^3. Dispersion was calculated on the basis of the total H_2 adsorption.

Temperature-programmed reduction (TPR) with H_2 was performed in a fixed-bed flow reactor. The TPR profile of each sample was recorded from room temperature to 973 K under a flow of 5.0% H_2/Ar at 30 ml/min, and the catalyst weight was 50 mg. The heating rate was 10 K/min. The consumption of H_2 was monitored continuously with TCD gas chromatograph equipped with a frozen acetone trap in order to remove H_2O from the effluent gas.The Ni *K*-, Pt L_3- and Ru *K*-edge EXAFS were measured at the BL-9C station of the Photon Factory at the High Energy Accelerator Research Organization in Tsukuba, Japan (Proposal no. 2004G280, 2006G095). The storage ring was operated at 2.5 GeV with a ring current of 300–450 mA. A Si(1 1 1) single crystal was used to obtain monochromatic X-ray beam. The monochromator was detuned to 60% of the maximum intensity to avoid higher harmonics in the X-ray beam. Two ion chambers filled with N_2 and 25% Ar diluted with N_2 for Ni *K*-edge EXAFS were used to detect I_0 and I, respectively. In the case of Pt L_3-edge EXAFS, N_2 and 15% Ar diluted with N_2 were used. Furthermore, in the case of Ru *K*-edge EXAFS, both ion chambers were filled with Ar. The samples for the EXAFS measurement were prepared by pressing catalyst powder of 15, 200 and 70 mg, and the thicknesses of the samples were chosen to be 0.1, 1.5 and 0.5 mm (10 mmϕ) to give edge jump of 0.5, 0.05 and 0.25 for Ni *K*-, Pt L_3- and Ru *K*-edge EXAFS, respectively. The samples were reduced with H_2 at 773 K for 0.5 h. After the pretreatment, the samples were transferred to the measurement cell without exposing the sample disk to air using a glove box filled with nitrogen. The samples after the temperature-programmed reduction (TPR) from room temperature to 550 K were also prepared and measured. The pretreatment conditions were the same as those of the TPR experiment. EXAFS data were collected in a transmission mode at room temperature. For EXAFS analysis, the oscillation was first extracted from the EXAFS data by a spline smoothing method [32]. The oscillation was normalized by the edge height around 50 eV. The Fourier transformation of the k^3-weighted EXAFS oscillation from k space to r space was performed to obtain a radial distribution function. The inversely Fourier filtered data were analyzed by a usual curve fitting method [33,34]. For the curve fitting analysis, the empirical phase shift and amplitude functions for the Pt–Pt bond was extracted from the data for Pt foil. Theoretical functions for the Pt–Ni bond were calculated using the FEFE8.2 program [35]. In the case of Ni *K*-edge EXAFS analysis, we used NiO as a model compound for the Ni–O and Ni–O–Ni bonds, and Ni foil for the Ni–Ni bond. For the Ru *K*-edge EXAFS analysis, Ru metal was used as a model compound for the Ru–Ru bond. The analysis of EXAFS data was performed using the "REX2000" program (RIGAKU Co. Version: 2.3.3).

3. Results and discussion

Fig. 1 shows catalytic performance in steam gasification of biomass over $Ni/CeO_2/Al_2O_3$, 12 wt.% $Ni/CeO_2/Al_2O_3$, $Ru/Ni/CeO_2/Al_2O_3$, $Rh/Ni/CeO_2/Al_2O_3$, $Pt/Ni/CeO_2/Al_2O_3$ after H_2 reduction. We carried out the activity test for 15 min. The formation rate of H_2, CO, CO_2 and CH_4 was observed, and their formation rates were almost stable during 15 min, although the coke deposition was observed as shown in Fig. 1. Generally speaking, coke deposition is one of the common and serious problems in the syngas production process [16–19]. The amount of coke is also represented by the weight ratio to the catalyst. The largest amount of coke was observed on 12 wt.% $Ni/CeO_2/Al_2O_3$ at the reaction temperature of 823 K, and this is determined to be 5 wt.%. In almost all cases, the coke amount was smaller than 5 wt.%. It is interpreted that the coke amount did not reach the level to cause the catalyst deactivation in the present cases. One example of the reaction time dependence has been shown in our previous report [31]. Therefore, the average formation rates of the products for 15 min are represented in the

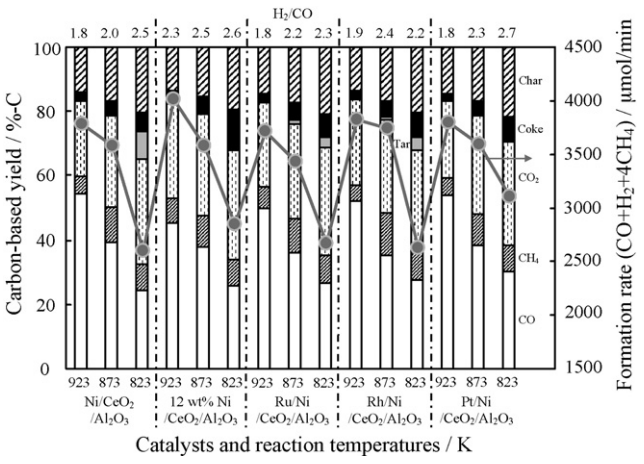

Fig. 1. Catalytic performance in steam gasification of biomass over the catalysts after H_2 reduction. Conditions: biomass, 60 mg/min (H_2O 9.2%, C 2191 μmol/min; H 3543 μmol/min; O 1475 μmol/min); N_2 flow rate, 60 ml/min (added H_2O)/C = 0.5 (steam flow rate 1110 μmol/min); reaction time, 15 min. H_2 reduction 773 K, 30 min. Loading amount: Ni 4 wt.%; Rh, Pt 0.1 wt.%; Ru 0.5 wt.%, when unindicated.

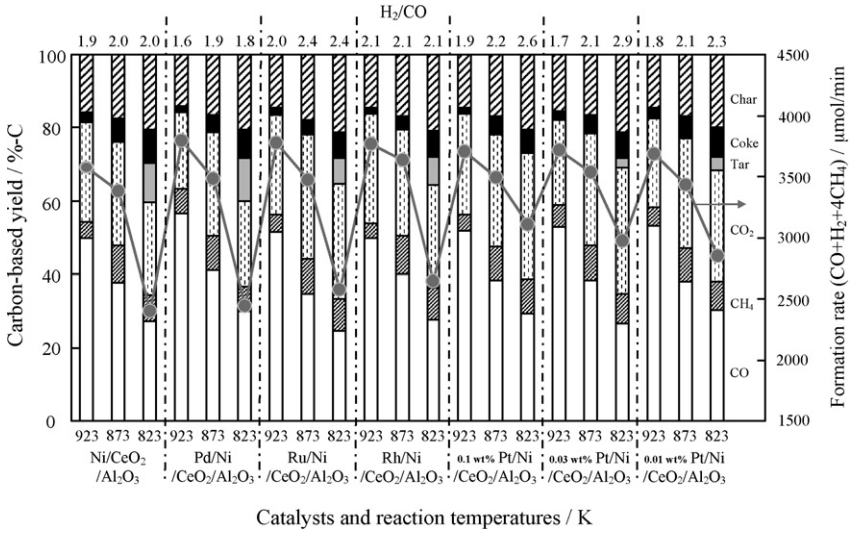

Fig. 2. Catalytic performance in steam gasification of biomass over the catalysts without H_2 reduction. Conditions: biomass, 60 mg/min (H_2O 9.2%, C 2191 μmol/min; H 3543 μmol/min; O 1475 μmol/min); N_2 flow rate, 60 ml/min (added H_2O)/C = 0.5 (steam flow rate 1110 μmol/min); reaction time, 15 min. Loading amount: Ni 4 wt.%; Pd, Rh 0.1 wt.%; Ru 0.5 wt.%, when unindicated.

results. From the comparison between $Ni/CeO_2/Al_2O_3$ and 12 wt.% $Ni/CeO_2/Al_2O_3$, especially at 823 K, the tar yield decreased with increasing the loading amount of Ni, on the contrary, the coke yield increased. Higher coke yield on the catalyst with larger loading amount of Ni can be related to the dispersion and particle size of Ni. According to the report on coke deposition in methane reforming, the rate of coke deposition was higher on Ni particles with larger particle size and lower dispersion [36]. The tendency of the present result is similar to that reported. In the experiments, the char did not contact with the catalysts, and the char yield is not dependent on the catalysts but on the reaction temperature. In addition, the effect of Pt addition was more effective than that of Rh and Ru. It should be noted that $Pt/Ni/CeO_2/Al_2O_3$ exhibited higher performance than 12 wt.% $Ni/CeO_2/Al_2O_3$ in terms of higher formation rate of the gaseous products and lower coke and tar yields, in particular at lower reaction temperature.

Fig. 2 shows catalytic performance in steam gasification of biomass over the catalysts without H_2 reduction. From the comparison between Figs. 1 and 2 regarding $Ni/CeO_2/Al_2O_3$, when the H_2 reduction pretreatment was omitted, the activity decreased significantly, especially at lower temperature. The order of the activity at 823 K over $Ni/CeO_2/Al_2O_3$ modified noble metals is as follows: $Pt \gg Rh > Ru > Pd$. In the case of 0.1 wt.% $Pt/Ni/CeO_2/Al_2O_3$, the tar yield was almost zero even at 823 K and without H_2 reduction. This result indicates that the promoting effect of Pt is most remarkable. Therefore, we also tested $Pt/Ni/CeO_2/Al_2O_3$ with smaller loading amount of Pt. The addition of very small amount of Pt such as 0.01 wt.% to the $Ni/CeO_2/Al_2O_3$ also enhanced the performance drastically. It should be noted that the performance of $Pt/Ni/CeO_2/Al_2O_3$ without H_2 reduction was almost the same as that with H_2 reduction, which means that the reactants can reduce the catalyst sufficiently, and that the H_2 reduction pretreatment becomes unnecessary.

Catalytic performance in steam gasification of biomass over CeO_2/Al_2O_3 supported noble metal catalysts without H_2 reduction is described in Fig. 3. It is clear that $M/CeO_2/Al_2O_3$ catalysts showed much lower performance than $Ni/CeO_2/Al_2O_3$ and those modified with noble metals. It has been known that noble metals can catalyze the steam reforming of hydrocarbons and biomass tars. Low activities of the $M/CeO_2/Al_2O_3$ catalysts can be explained by much smaller loading amount of noble metals than usual. This behavior indicates that main active species is Ni on the $M/Ni/CeO_2/Al_2O_3$ catalysts, and it is interpreted that the addition of Pt enhances the activity of Ni species over the $Pt/Ni/CeO_2/Al_2O_3$ catalysts.

Fig. 4 shows the effect of steam to carbon ratio on catalytic performance in steam gasification of biomass over $Ni/CeO_2/Al_2O_3$ and $Pt/Ni/CeO_2/Al_2O_3$ without H_2 reduction. On these

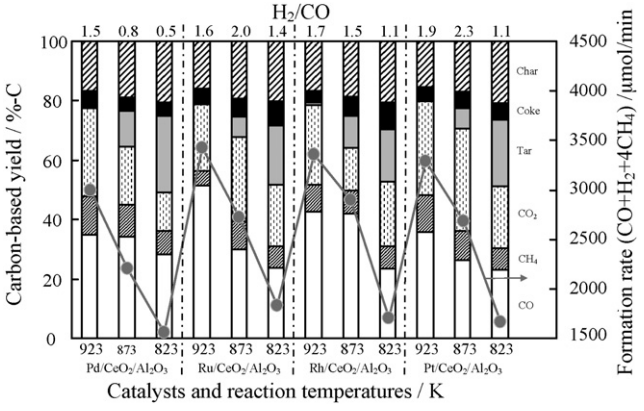

Fig. 3. Catalytic performance in steam gasification of biomass over the catalysts without H_2 reduction. Conditions: biomass, 60 mg/min (H_2O 9.2%, C 2191 μmol/min; H 3543 μmol/min; O 1475 μmol/min); N_2 flow rate, 60 ml/min (added H_2O)/C = 0.5 (steam flow rate 1110 μmol/min); reaction time, 15 min. Loading amount: Ni 4 wt.%; Pd, Rh, Pt 0.1 wt.%; Ru 0.5 wt.%, when unindicated.

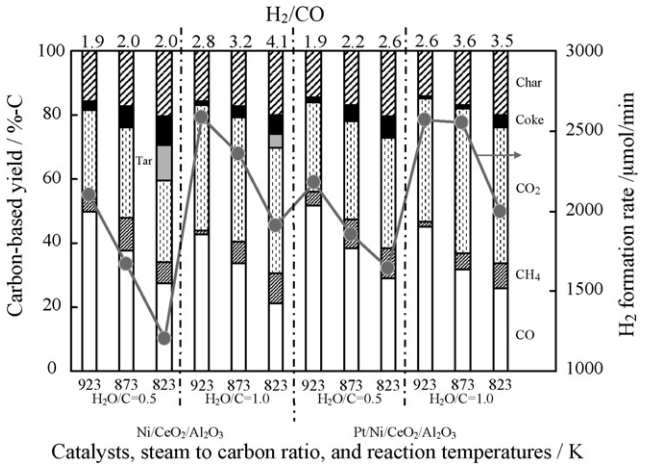

Fig. 4. Effect of steam to carbon ratio in steam gasification of biomass over Ni/CeO_2/Al_2O_3 and Pt/Ni/CeO_2/Al_2O_3 without H_2 reduction. Conditions: biomass, 60 mg/min (H_2O 9.2%, C 2191 μmol/min; H 3543 μmol/min; O 1475 μmol/min); N_2 flow rate, 60 ml/min (added H_2O)/C = 0.5, 1.0 (steam flow rate 1110, 2220 μmol/min); reaction time, 15 min. Loading amount: Ni 4 wt.%; Pt 0.1 wt.%, when unindicated.

two catalysts, the yield of coke and tar decreased with increasing the steam to carbon ratio from $H_2O/C = 0.5$ to 1.0. This tendency over Pt/Ni/CeO_2/Al_2O_3 was more remarkable than that over Ni/CeO_2/Al_2O_3. This can be related to the enhancement of the activity in tar reforming and coke gasification by increasing steam partial pressure. This can be connected to the suppression of coke deposition. The formation rate of H_2 and the yield of CO_2 increased, on the other hand, that of CO decreased. This behavior is associated with the water gas shift reaction ($CO + H_2O \rightarrow H_2 + CO_2$) under higher steam partial pressure ratio. This result also indicates that the catalysts can be contributed to the hydrogen production from biomass by steam gasification and reforming.

The amount of H_2 chemisorption on the catalysts after the reduction is listed in Table 1. The addition of all the noble metals enhanced the H_2 adsorption amount and the metal dispersion. This behavior has been observed on the Ni catalysts modified with noble metals [37,38]. The order of H_2 adsorption was as follows: Ru/Ni/CeO_2/Al_2O_3 > Rh/Ni/CeO_2/Al_2O_3 > 0.1 wt.% Pt/Ni/CeO_2/Al_2O_3 > Pd/Ni/CeO_2/Al_2O_3 > Ni/CeO_2/Al_2O_3. This tendency cannot explain higher activity of Pt/Ni/CeO_2/Al_2O_3, and the catalytic performance in steam gasification of biomass is not related to the H_2 adsorption amount.

Fig. 5(a) shows the TPR profiles of Ni/CeO_2/Al_2O_3 and those modified with noble metals. The H_2 consumption was observed in the range of 400–700 K over Ni/CeO_2/Al_2O_3, the reduction degree based on Ni content was beyond 100% as listed in Table 1, which is assigned to the reduction of CeO_2 ($CeO_2 + H_2 \rightarrow Ce_2O_3 + H_2O$). As reported previously [26], the H_2 consumption peak on Ni/CeO_2/Al_2O_3 can be due to the reduction of Ni interacted with CeO_2. The addition of Pt increased hydrogen consumption at 520 K, and decreased that at 620 K. On the other hand, the TPR profiles of CeO_2/Al_2O_3 supported noble metal catalysts are shown in Fig. 5(b), and no peaks were observed on the Pt/CeO_2/Al_2O_3 around 520 K. These profiles indicate that the peak at 520 K on Pt/Ni/CeO_2/Al_2O_3 can be assigned to the reduction of NiO promoted by the Pt addition. From the comparison between M/Ni/CeO_2/Al_2O_3 and M/CeO_2/Al_2O_3 (M = Rh, Ru and Pd) in the TPR profiles, it is suggested that the lower temperature peak can be assigned to the reduction of CeO_2 promoted by the presence of Rh, Ru and Pd, and these behaviors are different from the case of Pt. These results suggest that Pt tends to interact with NiO species, and other noble metals tend to interact with CeO_2. This interaction between Pt and Ni species can enhance the performance in the steam gasification of biomass. In addition, the peak intensity near 520 K in the TPR profiles on Pt/Ni/CeO_2/Al_2O_3 decreased

Table 1
Results of H_2 adsorption and TPR of various catalysts

Catalysts	BET surface area ($m^2\ g^{-1}$-cat.)	Loading amount				H_2 adsorption[a] (10^{-5} mol g^{-1}-cat.)	Dispersion[b] (%)	H_2 consumption[c] (10^{-3} mol g^{-1}-cat.)	Ni-based reduction degree[d] (%)
		Ni		Noble metal					
		wt.%	10^{-3} mol g^{-1}-cat.	wt.%	10^{-5} mol g^{-1}-cat.				
Ni/CeO_2/Al_2O_3	15	4	0.68	0	0	4.0	5.8	1.02	149
	18	12	2.04	0	0	8.4	4.1	–	–
Pt/Ni/CeO_2/Al_2O_3	15	4	0.68	0.1	0.51	5.7	8.4	0.97	142
	14	4	0.68	0.03	0.15	5.6	8.2	0.94	138
	15	4	0.68	0.01	0.05	5.5	8.1	0.92	133
Rh/Ni/CeO_2/Al_2O_3	16	4	0.68	0.1	0.97	6.1	9.0	1.0	144
Ru/Ni/CeO_2/Al_2O_3	15	4	0.68	0.5	5.0	6.2	9.0	1.1	146
Pd/Ni/CeO_2/Al_2O_3	18	4	0.68	0.1	0.94	5.5	8.0	0.95	138
Pt/CeO_2/Al_2O_3	17	0	0	0.1	0.51	–	–	0.32	–
Rh/CeO_2/Al_2O_3	17	0	0	0.1	0.97	–	–	0.37	–
Ru/CeO_2/Al_2O_3	19	0	0	0.5	5.0	–	–	0.45	–
Pd/CeO_2/Al_2O_3	17	0	0	0.1	0.94	–	–	0.32	–

[a] Total hydrogen adsorption at 298 K.
[b] 2(H_2 adsorption)/(Ni + Noble metals) × 100.
[c] H_2 consumption in TPR profiles shown in Fig. 3.
[d] Based on the assumption that $Ni^{2+} + H_2 \rightarrow Ni^0 + 2H^+$, and the contribution of noble metals were neglected.

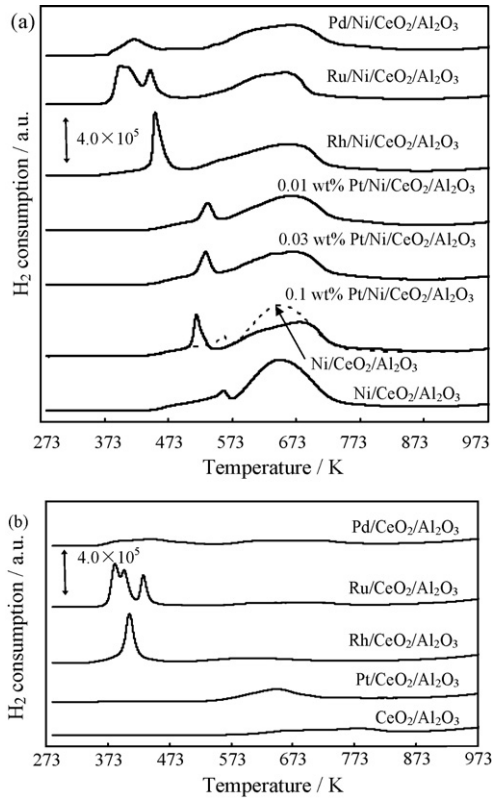

Fig. 5. TPR profiles of the catalysts. (a) M/Ni/CeO_2/Al_2O_3 and (b) M/CeO_2/Al_2O_3 (M = Pt, Rh, Ru, Pd). TPR conditions: heating rate 10 K/min, room temperature to 973 K, 5% H_2/Ar: 30 ml/min, Sample weight: 50 mg-cat. Broken line represents a TPR profile of Ni/CeO_2/Al_2O_3 for the comparison. Loading amount: Ni 4 wt.%; Pd, Rh, Pd 0.1 wt.%; Ru 0.5 wt.%, when unindicated.

gradually with decreasing the loading amount of Pt from 0.1 to 0.01 wt.%, and this behavior can be related to the catalytic performance in steam gasification. On the other hand, regarding the broad peak in the temperature range of 570–750 K, the peak top was located at 650 and 690 K on Ni/CeO_2/Al_2O_3 and 0.1 wt.% Pt/Ni/CeO_2/Al_2O_3, respectively. It appears that this broad peak is shifted to a 40 K higher temperature by the addition of Pt to Ni/CeO_2/Al_2O_3. For the comparison, the TPR profile of Ni/CeO_2/Al_2O_3 is plotted at that of 0.1 wt.% Pt/Ni/CeO_2/Al_2O_3. This comparison indicates that the change of the peak top position by the Pt addition is explained by the shift of the lower temperature part (570–680 K) in the broad peak to the sharp peak at 520 K observed on 0.1 wt.% Pt/Ni/CeO_2/Al_2O_3. The area of the shifted part corresponds to 25% of the total area. This means that the reduction of considerable amount of Ni is promoted by a small amount of Pt. This promoting effect can be explained by hydrogen spillover phenomenon [39,40]. The Ni species, whose reduction was promoted by Pt addition, can be positioned in the region where the spillover hydrogen can reach. These results also support that the interaction between Pt and Ni species plays important roles on the high activity in the steam gasification of biomass.

Fig. 6 shows the results of Pt L_3-edge and Ru K-edge EXAFS of Pt/Ni/CeO_2/Al_2O_3 and Ru/Ni/CeO_2/Al_2O_3 after H_2 reduction at 773 K. Curve fitting results are listed in Table 2. In the FT spectra in Fig. 6(b), the peak of Pt/Ni/CeO_2/Al_2O_3 was observed at about 0.21 nm, and it is obviously shorter than the Pt–Pt bond in Pt foil. Therefore, the EXAFS of Pt/Ni/CeO_2/Al_2O_3 was fitted by the Pt–Ni bond. The obtained bond length of the Pt–Ni bond was also much shorter than that of the intermetallic compound between Pt and Ni (NiPt) [41]. The distance of the Pt–Pt and Pt–Ni bonds of the bulk NiPt is 0.277 and 0.269 nm, respectively. This disagreement indicates that the intermetallic compound (NiPt) are not formed on the catalyst. The bond length of Pt–Ni is nearly equal to that of the Ni–Ni bond (0.249 nm) in Ni metal as listed in Table 3 as a reference. This similarity suggests the formation of Pt–Ni alloy phase. The Pt atoms can partly substitute Ni atoms in Ni metal phase. These structural properties are supported by the previous reports on the alloy formation of Pt–Ni [38,42–45]. In addition, the Pt–Pt bond is not detected in the EXAFS analysis of Pt/Ni/CeO_2/Al_2O_3 at all, which suggests that Pt and Ni are mixed well in the alloy phase. Considering that the coordination number (CN) of the Pt–Ni bond is smaller than that of the bulk of the fcc metal (CN = 12), it is suggested that the Pt atoms are located preferentially on the near-surface of the metal particles. In contrast, in the case of Ru/Ni/CeO_2/Al_2O_3, the FT peak position was almost the same as that of the Ru metal. In fact, the Ru K-edge EXAFS of Ru/Ni/CeO_2/Al_2O_3 was fitted well by the Ru–Ru bond originated from the Ru metal, and it is indicated that major part of Ru atoms did not interact with Ni and Ru metal particles were formed.

Fig. 7 shows the results of Ni K-edge EXAFS analysis of three Ni catalysts modified with Ru, Rh and Pt after the H_2 reduction at 773 K. The curve fitting results are listed in Table 3. All the peaks at around 0.21 nm shown in Fig. 7(b) can be assigned to the Ni–Ni bond clearly. Based on the curve fitting results, it is found that the CN of the Ni–Ni bond on Pt/Ni/

Table 2
Curve fitting results of Pt L_3- and Ru K-edge EXAFS of the catalysts after the reduction at 773 K

Catalysts	Shells	CN[a]	R[b] (10^{-1} nm)	σ[c] (10^{-1} nm)	ΔE_0[d] (eV)	R_f[e] (%)
Pt/Ni/CeO_2/Al_2O_3	Pt–Ni	7.3 ± 0.3	2.52 ± 0.003	0.087 ± 0.004	3.7 ± 0.5	0.5
Ru/Ni/CeO_2/Al_2O_3	Ru–Ru	7.2 ± 0.2	2.66 ± 0.001	0.077 ± 0.002	−4.3 ± 0.4	1.0

Fourier transform range: 30–128 nm^{-1}, Fourier filtering range: 0.160–0.267 nm (Pt/Ni/CeO_2/Al_2O_3), 0.190–0.295 nm (Ru/Ni/CeO_2/Al_2O_3).
[a] Coordination number.
[b] Bond distance.
[c] Debye–Waller factor.
[d] Difference in the origin of photoelectron energy between the reference and the sample.
[e] Residual factor.

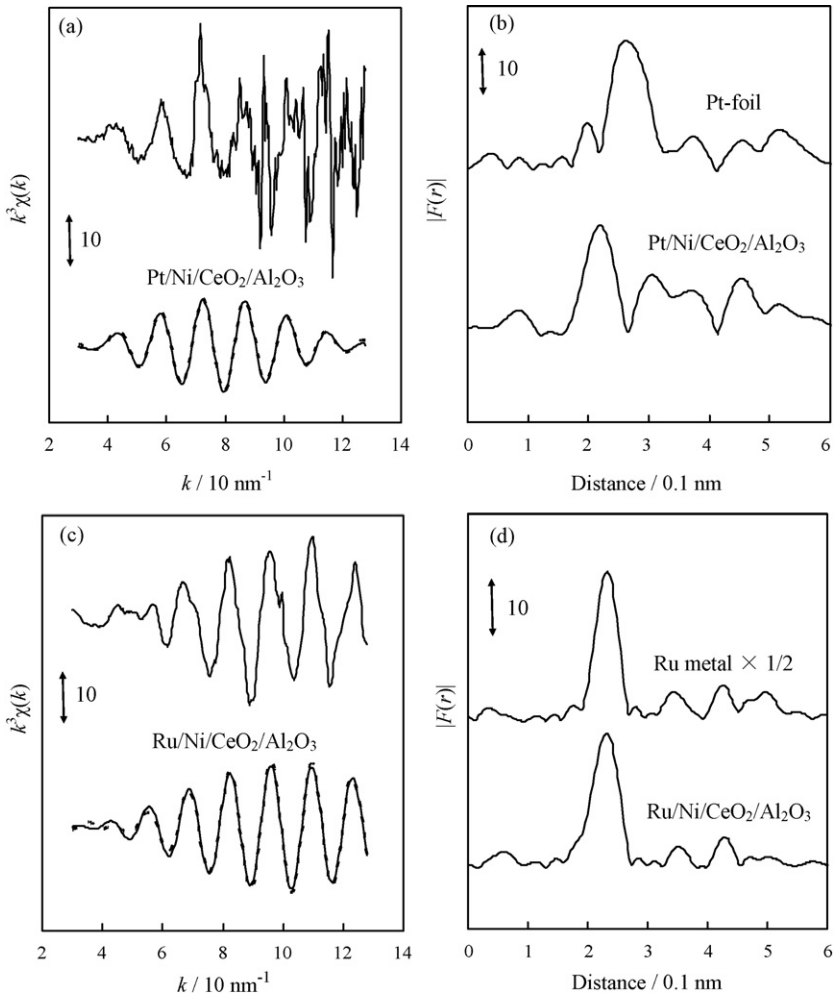

Fig. 6. Results of Pt L_3- and Ru K-edge EXAFS analysis of the catalysts reduced at 773 K. (a) k^3-weighted EXAFS oscillations, Fourier filtered EXAFS data (solid line), and calculated data (dotted line). Fourier filtering range: 0.160–0.267 nm. (b) Fourier transforms of k^3-weighted Pt L_3-edge EXAFS, FT range: 30–128 nm^{-1}. (c) k^3-weighted EXAFS oscillations, Fourier filtered EXAFS data (solid line), and calculated data (dotted line). Fourier filtering range: 0.160–0.267 nm. (d) Fourier transforms of k^3-weighted Ru K-edge EXAFS, FT range: 30–128 nm^{-1}.

CeO_2/Al_2O_3 was smaller than that on other two catalysts. On the other hand, according to Table 1, three catalysts gave almost the same metal dispersion, which cannot explain low CN of Pt/$Ni/CeO_2/Al_2O_3$. On the other hand, the Pt–Ni bond was observed in the Pt L_3-edge EXAFS result, and this suggests the presence of the Ni–Pt bond, which is difficult to detect the contribution by Ni K-edge EXAFS because of low molar ratio of Pt/Ni = 1/75. However, the substitution of Ni with Pt by alloying can increase the distortion in the Ni metal lattice [46] and this phenomenon can apparently decrease the CN on Pt/Ni/CeO_2/Al_2O_3. In contrast, in the case of $Ru/Ni/CeO_2/Al_2O_3$ and $Rh/Ni/CeO_2/Al_2O_3$, this kind of contribution is much smaller.

Table 3
Curve fitting results of Ni K-edge EXAFS of Ni catalysts after the reduction at 773 K

Catalysts	Shells	CN[a]	R^b (10^{-1} nm)	σ^c (10^{-1} nm)	$\Delta E_0{}^d$ (eV)	$R_f{}^e$ (%)
$Pt/Ni/CeO_2/Al_2O_3$	Ni–Ni	8.9 ± 0.2	2.49 ± 0.002	0.075 ± 0.003	0.5 ± 0.4	1.0
$Rh/Ni/CeO_2/Al_2O_3$	Ni–Ni	10.3 ± 0.2	2.49 ± 0.001	0.064 ± 0.002	−0.6 ± 0.3	0.1
$Ru/Ni/CeO_2/Al_2O_3$	Ni–Ni	10.1 ± 0.2	2.49 ± 0.001	0.068 ± 0.002	−0.4 ± 0.3	0.1
Ni foil	Ni–Ni	12	2.49	0.060	0.0	

Fourier transform range: 30–160 nm^{-1}, Fourier filtering range: 0.150–0.279 nm.
[a] Coordination number.
[b] Bond distance.
[c] Debye–Waller factor.
[d] Difference in the origin of photoelectron energy between the reference and the sample.
[e] Residual factor.

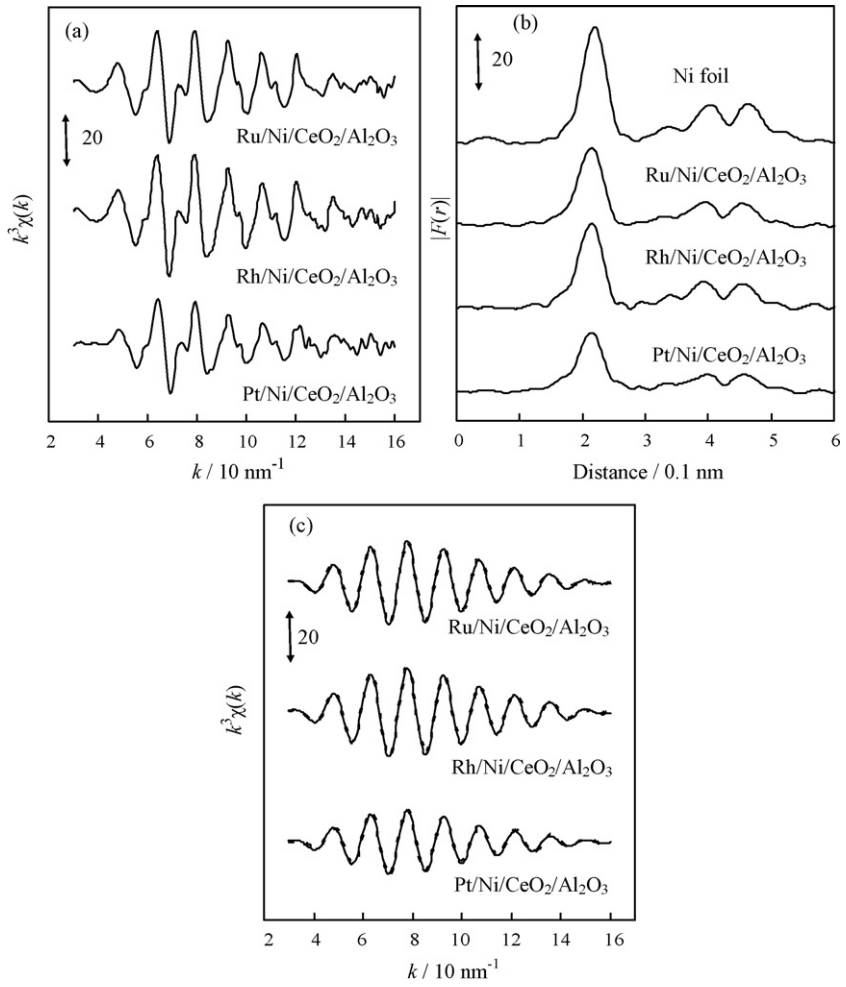

Fig. 7. Results of Ni *K*-edge EXAFS analysis of the catalysts reduced at 773 K. (a) k^3-weighted EXAFS oscillations. (b) Fourier transforms of k^3-weighted Ni *K*-edge EXAFS, FT range: 30–160 nm^{-1}. (c) Fourier filtered EXAFS data (solid line) and calculated data (dotted line). Fourier filtering range: 0.150–0.279 nm.

Table 4
Curve fitting results of Ni *K*-edge EXAFS of the catalysts after the temperature-programmed reduction from room temperature to 550 K

Catalysts	Shells	CN[a]	R[b] (10^{-1} nm)	σ[c] (10^{-1} nm)	ΔE_0[d] (eV)	R_f[e] (%)
$Pt/Ni/CeO_2/Al_2O_3$	Ni–Ni	4.7 ± 0.6	2.46 ± 0.009	0.073 ± 0.010	−6.9 ± 3.3	1.0
	Ni–O	1.6 ± 0.6	2.08 ± 0.003	0.085 ± 0.038	−9.0 ± 5.7	
	Ni–O–Ni	6.1 ± 0.9	2.94 ± 0.008	0.090 ± 0.010	−0.2 ± 1.7	
$Rh/Ni/CeO_2/Al_2O_3$	Ni–Ni	1.2 ± 0.4	2.46 ± 0.009	0.080 ± 0.020	−5.5 ± 2.8	0.3
	Ni–O	4.7 ± 0.6	2.09 ± 0.008	0.073 ± 0.010	2.6 ± 1.5	
	Ni–O–Ni	8.7 ± 0.3	2.94 ± 0.002	0.075 ± 0.002	−1.7 ± 0.4	
$Ru/Ni/CeO_2/Al_2O_3$	Ni–O	5.7 ± 0.5	2.09 ± 0.007	0.077 ± 0.010	7.8 ± 1.5	0.5
	Ni–O–Ni	9.7 ± 0.3	2.94 ± 0.002	0.078 ± 0.003	−1.5 ± 0.4	
Ni foil	Ni–Ni	12	2.49	0.060	0.0	
NiO	Ni–O	6	2.09	0.060	0.0	
	Ni–O–Ni	12	2.94	0.060		

Fourier transform range: 30–160 nm^{-1}, Fourier filtering range: 0.150–0.279 nm.
[a] Coordination number.
[b] Bond distance.
[c] Debye–Waller factor.
[d] Difference in the origin of photoelectron energy between the reference and the sample.
[e] Residual factor.

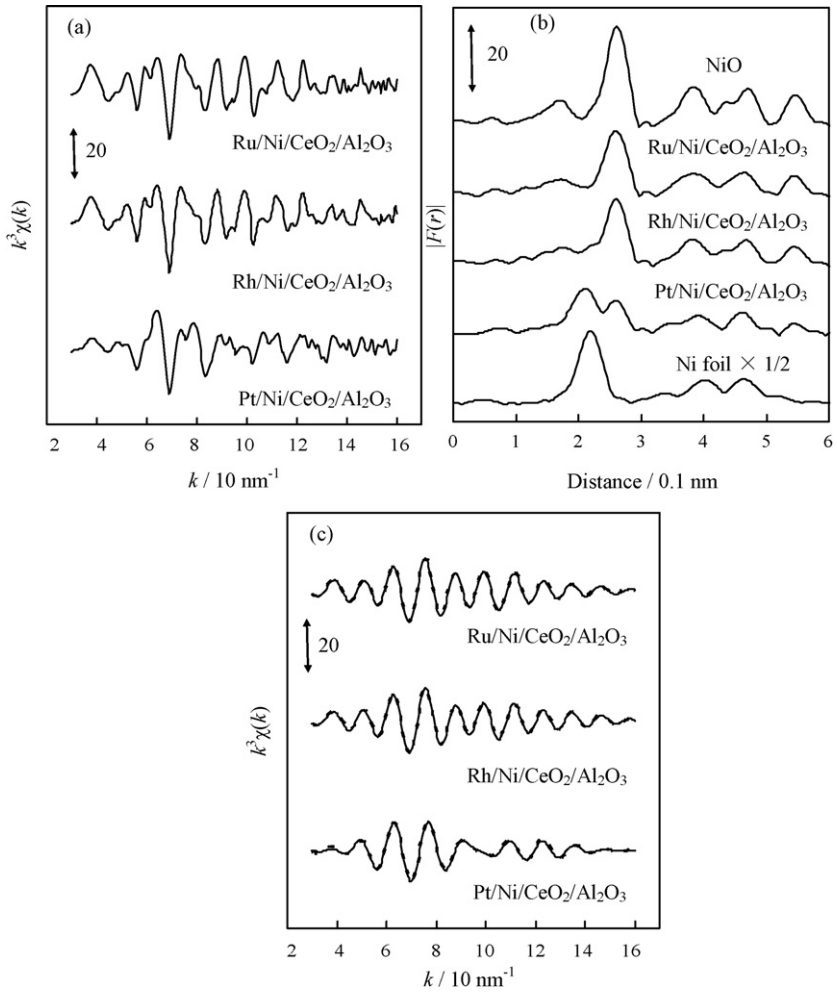

Fig. 8. Results of Ni *K*-edge EXAFS analysis of the catalysts after the temperature-programmed reduction from room temperature to 550 K. (a) k^3-weighted EXAFS oscillations. (b) Fourier transforms of k^3-weighted Ni *K*-edge EXAFS, FT range: 30–160 nm^{-1}. (c) Fourier filtered EXAFS data (solid line) and calculated data (dotted line). Fourier filtering range: 0.132–0.322 nm.

From the TPR results shown above, it is found that the reduction profile of $Pt/Ni/CeO_2/Al_2O_3$ is also different from those of two other catalysts. In order to confirm the suggestion from TPR, we also measured the Ni *K*-edge EXAFS of the catalysts after the TPR from room temperature to 550 K (Fig. 8). The curve fitting results are listed in Table 4. In the case of $Ru/Ni/CeO_2/Al_2O_3$ and $Rh/Ni/CeO_2/Al_2O_3$, the main FT peak is assigned to the Ni–O–Ni bond in NiO. This indicates that the major part of Ni species on $Ru/Ni/CeO_2/Al_2O_3$ and $Rh/Ni/CeO_2/Al_2O_3$ is not reduced at 550 K. In contrast, the peak at around 0.21 nm assigned to the Ni–Ni bond in Ni metal was observed over $Pt/Ni/CeO_2/Al_2O_3$, as shown in Fig. 8(b) and Table 4. In addition, the CNs of Ni–O and Ni–O–Ni over $Pt/Ni/CeO_2/Al_2O_3$ are much smaller than those over $Rh/Ni/CeO_2/Al_2O_3$ and $Ru/Ni/CeO_2/Al_2O_3$. This result suggests that considerable amount of Ni on the $Pt/Ni/CeO_2/Al_2O_3$ is reduced up to 550 K. The results and their interpretation in the TPR part are supported. This difference between Pt and other noble metals can be explained by their affinity to CeO_2. The affinity of noble metals with CeO_2 has been reported for the CeO_2 supported noble metal catalysts with the loading amounts larger than in the present case. The affinity of Pt with CeO_2 is also lower than that of other noble metals [47]. It is thought that this tendency is more significant for the catalysts with smaller loading amounts. At present, the reason why Pt is superior to other noble metals as an additive to $Ni/CeO_2/Al_2O_3$ is not elucidated sufficiently, and further investigations are necessary. The strong interaction of noble metals with CeO_2 suppresses their interaction with Ni species.

According to the results reported previously, the addition of noble metals such as Rh and Pd to Ni catalysts enhanced the performance in the reforming of methane and the alloying of the noble metals with Ni has been also confirmed [37,48–52]. These results suggest that high activity is available if the added noble metal is alloyed with Ni. Based on the EXAFS and TPR results, added Rh, Ru and Pd did not form the alloy with Ni, and the promoting effect was not so remarkable as that by Pt.

4. Conclusions

Additive effect of noble metals such as Pt, Pd, Rh and Ru to $Ni/CeO_2/Al_2O_3$ catalysts prepared by the co-impregnation

method was investigated in the steam gasification of biomass. The addition of Pt was much more effective than Rh, Ru and Pd. In particular, the $Pt/Ni/CeO_2/Al_2O_3$ catalyst without H_2 reduction treatment exhibited similar level of the performance to that after the H_2 reduction pretreatment. This behavior indicates that the catalyst can be activated easily with the compounds contained in the tar. The TPR profiles suggest that the Pt species can interact with Ni species much more strongly than other noble metals. In addition, the EXAFS analysis showed the presence of the Pt–Ni bond, and Pt–Ni alloy formation. In contrast, the alloy formation of Ni with Ru and Rh was not clearly confirmed. These characterization results suggest that high performance of $Pt/Ni/CeO_2/Al_2O_3$ can be due to the strong interaction between Pt and Ni to form the alloy.

Acknowledgements

A part of this research was supported by Fukuoka Strategy Conference for Hydrogen Energy and Nippon Steel Corporation.

References

[1] A.V. Bridgwater, Appl. Catal. A: Gen. 116 (1994) 5.
[2] L. Devi, K.J. Ptasinski, F.J.J.G. Janssen, Biomass Bioenergy 24 (2003) 125.
[3] D. Sutton, B. Kelleher, J.R.H. Ross, Fuel Proc. Technol. 73 (2001) 155.
[4] K. Tomishige, M. Asadullah, K. Kunimori, Catal. Today 89 (2004) 389.
[5] M. Asadullah, K. Tomishige, K. Fujimoto, Catal. Commun. 2 (2001) 63.
[6] M. Asadullah, S. Ito, K. Kunimori, M. Yamada, K. Tomishige, J. Catal. 208 (2002) 255.
[7] M. Asadullah, S. Ito, K. Kunimori, M. Yamada, K. Tomishige, Environ. Sci. Technol. 36 (2002) 4476.
[8] M. Asadullah, T. Miyazawa, S. Ito, K. Kunimori, K. Tomishige, Appl. Catal. A: Gen. 246 (2003) 103.
[9] M. Asadullah, T. Miyazawa, S. Ito, K. Kunimori, M. Yamada, K. Tomishige, Appl. Catal. A: Gen. 255 (2003) 169.
[10] M. Asadullah, T. Miyazawa, S. Ito, K. Kunimori, S. Koyama, K. Tomishige, Biomass Bioenergy 26 (2004) 269.
[11] M. Asadullah, T. Miyazawa, S. Ito, K. Kunimori, M. Yamada, K. Tomishige, Appl. Catal. A: Gen. 267 (2004) 95.
[12] K. Tomishige, T. Miyazawa, T. Kimura, K. Kunimori, Catal. Commun. 6 (2005) 37.
[13] K. Tomishige, T. Miyazawa, T. Kimura, K. Kunimori, N. Koizumi, M. Yamada, Appl. Catal. B: Environ. 60 (2005) 299.
[14] M. Asadullah, T. Miyazawa, S. Ito, K. Kunimori, K. Tomishige, Energy Fuels 17 (2003) 842.
[15] K. Tomishige, T. Miyazawa, M. Asadullah, S. Ito, K. Kunimori, J. Jpn. Petrol. Inst. 46 (2003) 322.
[16] K. Tomishige, Y. Himeno, Y. Matsuo, Y. Yoshinaga, Y. Fujimoto, Ind. Eng. Chem. Res. 39 (2000) 1891.
[17] K. Tomishige, Y.G. Chen, K. Fujimoto, J. Catal. 181 (1999) 91.
[18] O. Yamazaki, K. Tomishige, K. Fujimoto, Appl. Catal. A: Gen. 136 (1996) 49.
[19] C.H. Bartholomew, Catal. Rev. Sci. Eng. 24 (1982) 67.
[20] D. Wang, D. Montane, E. Chornet, Appl. Catal. A: Gen. 143 (1996) 245.
[21] D.N. Bangala, N. Abatzoglou, E. Chornet, AICHE J. 44 (1998) 927.
[22] R. Coll, J. Salvado, X. Ferriol, D. Montane, Fuel Process. Technol. 74 (2001) 19.
[23] T. Furusawa, A. Tsutsumi, Appl. Catal. A: Gen. 278 (2005) 207.
[24] T. Furusawa, A. Tsutsumi, Appl. Catal. A: Gen. 278 (2005) 195.
[25] S. Rapagna, N. Jand, A. Kiennemann, P.U. Foscolo, Biomass Bioenergy 19 (2000) 187.
[26] R. Martinez, E. Romero, L. Garcia, R. Bilbao, Fuel Process. Technol. 85 (2003) 201.
[27] L. Garcia, A. Benedicto, E. Romeo, M.L. Salvador, J. Arauzo, R. Bilbao, Energy Fuels 16 (2002) 1222.
[28] T. Miyazawa, T. Kimura, J. Nishikawa, S. Kado, K. Kunimori, K. Tomishige, Catal. Today 115 (2006) 254.
[29] J. Nishikawa, T. Miyazawa, K. Nakamura, M. Asadullah, K. Kunimori, K. Tomishige, Catal. Commun. 9 (2008) 195.
[30] K. Tomishige, T. Kimura, J. Nishikawa, T. Miyazawa, K. Kunimori, Catal. Commun. 8 (2007) 1074.
[31] T. Kimura, T. Miyazawa, J. Nishikawa, T. Miyao, S. Naito, K. Okumura, K. Kunimori, K. Tomishige, Appl. Catal. B: Environ. 68 (2006) 160.
[32] J.W. Cook, D.E. Sayers, J. Appl. Phys. 52 (1981) 5024.
[33] K. Okumura, J. Amano, N. Yasunobu, M. Niwa, J. Phys. Chem. B 104 (2000) 1050.
[34] K. Okumura, S. Matsumoto, N. Nishiaki, M. Niwa, Appl. Catal. B: Environ. 40 (2003) 151.
[35] A.L. Ankudinov, B. Ravel, J.J. Rehr, S.D. Conradson, Phys. Rev. B 58 (1998) 7565.
[36] Y. Chen, K. Tomishige, K. Yokoyama, K. Fujimoto, J. Catal. 184 (1999) 479.
[37] M. Nurunnabi, Y. Mukainakano, S. Kado, B.T. Li, K. Kunimori, K. Suzuki, K. Fujimoto, K. Tomishige, Appl. Catal. A: Gen. 299 (2006) 145.
[38] M. Nurunnabi, B.T. Li, K. Kunimori, K. Suzuki, K. Fujimoto, K. Tomishige, Appl. Catal. A: Gen. 292 (2005) 272.
[39] K. Tomishige, A. Okabe, K. Fujimoto, Appl. Catal. A: Gen. 194 (2000) 383.
[40] R. Ueda, T. Kusakari, K. Tomishige, K. Fujimoto, J. Catal. 194 (2000) 14.
[41] A. Jentys, G.L. Haller, J.A. Lercher, J. Phys. Chem. 97 (1993) 484.
[42] A.S. Bommannavar, P.A. Montano, M.J. Yacamn, Surf. Sci. 156 (1985) 426.
[43] Y.G. Chen, K. Tomishige, K. Yokoyama, K. Fujimoto, Appl. Catal. A: Gen. 165 (1997) 335.
[44] B.T. Li, S. Kado, Y. Mukainakano, T. Miyazawa, T. Miyao, S. Naito, K. Okumura, K. Kunimori, K. Tomishige, J. Catal. 245 (2007) 144.
[45] B.T. Li, S. Kado, Y. Mukainakano, M. Nurunnabi, T. Miyao, S. Naito, K. Kunimori, K. Tomishige, Appl. Catal. A: Gen. 304 (2006) 62.
[46] K. Tomishige, K. Asakura, Y. Iwasawa, J. Catal. 149 (1994) 70.
[47] S. Hosokawa, M. Taniguchi, K. Utani, H. Kanai, S. Imamura, Appl. Catal. A: Gen. 289 (2005) 115.
[48] Y. Mukainakano, B. Li, S. Kado, T. Miyazawa, K. Okumura, T. Miyao, S. Naito, K. Kunimori, K. Tomishige, Appl. Catal. A: Gen. 318 (2007) 252.
[49] M. Nurunnabi, Y. Mukainakano, S. Kado, K. Kunimori, K. Tomishige, Chem. Lett. 35 (2006) 1072.
[50] M. Nurunnabi, Y. Mukainakano, S. Kado, T. Miyazawa, K. Okumura, T. Miyao, S. Naito, K. Fujimoto, K. Suzuki, K. Kunimori, K. Tomishige, Appl. Catal. A: Gen. 308 (2006) 1.
[51] M. Nurunnabi, S. Kado, K. Suzuki, K. Fujimoto, K. Tomishige, K. Kunimori, Catal. Commun. 7 (2006) 488.
[52] M. Nurunnabi, K. Fujimoto, K. Suzuki, B.T. Li, S. Kado, K. Kunimori, K. Tomishige, Catal. Commun. 7 (2006) 73.